The Statistical Distributions and Evolutions of Seeing Values

R Racine
Association of Canadian Universities for Research in Astronomy & Département de physique, Université de Montréal, CP 6128, Succ. Centre-Ville, Montreal H3C-3J7, Canada

E-mail: racine@astro.umontreal.ca

Abstract. Extensive series of DIMM and MASS seeing values from thirteen astronomical sites are used to examine the shapes of their statistical distributions and their evolutions with time. At all sites, the distributions of seeing values can be satisfactorily reproduced over densities that span more than four orders of magnitude by random combinations of seeing values from two independent equal-population log-normal seeing components. The seeing varies typically by a factor of 4 throughout a night. At good sites, it reaches sub-half-arc second on 80% of the night. It is most stable when near its modal value where the delays for a 10% change in DIMM seeing average ~50 minutes. The average delays are ~25 minutes at the 10^{th} and 90^{th} percentiles of the distributions. These lifetimes differ by a factor of 4 between the fastest and the slowest seeing sites. The MASS seeing evolves ~7 times faster than the DIMM seeing. These characteristics make forecasting seeing a tall challenge.

1. Introduction

Much literature discusses the techniques for and the results of optical turbulence measurements above astronomical sites. Here we examines a relatively obscure sub-topic: the *shape* of the seeing values distributions, i.e. of the distributions of the full widths at half maximum intensity ε_0 imposed by atmospheric optical turbulence to stellar point spread functions. The evolutions with time of the seeing values are also examined, as this is of interest in planning seeing-critical astronomical observations and also in measuring the challenges of seeing forecasting using climate models. Seeing values are inferred from differential image motion monitor (DIMM) [1] and multi-aperture scintillation sensor (MASS) [2] observations assuming Kolmogorov turbulence of infinite outer scale L_0. MASS and DIMM are usually operated together on a same mount. Seeing is traditionally expressed in second of arc (") at a wavelength of 500 nm at the zenith.

2. Seeing distributions

The data used are years-long web-accessible archival series of ε_0 values obtained at thirteen sites. The measurements, averaged over 1 minute, were all made from elevations of about 7 m above local ground. For each site, the differential density distribution values were compiled in successive intervals in ε_0 that are multiples of 0.01" wide.

To model the distributions, numerical Monte-Carlo (MC) simulations adding in 5/3 power 140 000 pairs of ε_0 values randomly drawn from two independent distributions of same populations and adjustable medians (μ_1, μ_2) and dispersions (σ_1, σ_2) were run and the process was iterated until the

least χ^2 fit of the resulting distribution to the data was obtained. In a first pass through the data the two model distributions had the form of log-normals but the powers *n* of the arguments of the exponentials, which are 2 for log-normals, were left as free fit parameters. This allowed testing if log-normals yield appropriate representations. This was confirmed, the values of *n* returned by the fits averaging 2.02 with a dispersion of 0.04. Final fits with log-normals were then adopted.

The results of the exercise are summarized in table 1. Column 1 identifies the sites and their altitudes. Columns 2, 3 and 4, 5 give the medians and the logarithmic dispersions of the DIMM and MASS ε_0 data. Columns 6, 7 and 8, 9 give the values of the medians and dispersions μ_1, σ_1 and μ_2, σ_2 respectively of the log-normal components whose combinations best fit the DIMM ε_0 distributions and column 10 gives the χ^2 per degrees of freedom of these fits. The two components have quite different dispersions and are accordingly termed the "narrow DIMM components" and "wide DIMM components". Columns 11 through 15 contain analogous results for fits to the MASS distributions which are improved by adding the effects of "weak MASS components" to those of "strong MASS components".

Table 1. Characteristics of Seeing Distributions and of their Components.

1		2	3	4	5	6	7	8	9	10	11	12	13	14	15
Site	Altitude (m)	$<\varepsilon_0>$ (asec.) / dispersion				narrow DIMM component		wide DIMM component		χ^2	weak MASS component		strong MASS component		χ
		DIMM	σ	MASS	σ	μ_1 (")	σ_1	μ_2 {")	σ_2		μ_3 (")	σ_3	μ_4 (")	σ_4	
Mauna Kea, Hawai'i															
13N	4040	0.74	0.46	0.33	0.68	0.36	0.30	0.56	0.66	4.8	0.15	0.64	0.23	0.93	4.2
MKAM	4200	0.64	0.42	0.38	0.59	0.30	0.30	0.48	0.62	5.3	0.04	0.68	0.37	0.74	8.9
UH 2.2-m[1]	4200	0.65	0.33	--	--	0.50	0.27	0.30	0.71	2.4	--	--	--	--	--
Chile, Norte Grande															
Tolar	2290	0.63	0.36	0.44	0.51	0.36	0.26	0.44	0.60	0.0	0.20	0.88	0.30	0.49	17.1
Paranal	2640	0.87	0.41	0.43	0.47	0.31	0.25	0.67	0.55	3.5	0.13	0.21	0.41	0.53	6.0
Armazones	3060	0.65	0.40	0.42	0.52	0.32	0.31	0.50	0.55	1.8	0.18	0.65	0.31	0.69	17.6
Tolonchar	4480	0.64	0.35	0.47	0.57	0.36	0.27	0.45	0.56	1.1	0.07	0.85	0.45	0.58	14.8
Chile, Norte Chico															
Tololo	2210	0.86	0.39	0.64	0.50	0.48	0.22	0.62	0.65	1.3	0.08	0.23	0.63	0.54	6.4
Vizcachas	2050	0.86	0.34	0.42	0.49	0.48	0.08	0.55	0.53	7.5	0.16	0.32	0.34	0.60	16.8
Pachon	2850	0.76	0.34	0.42	0.52	0.49	0.27	0.48	0.60	8.4	0.12	0.82	0.36	0.60	15.7
North America															
Palomar	1710	1.11	0.38	0.43	0.63	0.69	0.21	0.74	0.66	0.8	0.09	0.45	0.44	0.70	4.2
SPM	2830	0.79	0.46	0.38	0.66	0.40	0.24	0.60	0.68	0.5	0.08	0.37	0.35	0.72	4.4
Islas Canarias															
ORM	2396	0.78	0.44	0.31	0.56	0.45	0.22	0.55	0.75	3.2	0.11	0.33	0.27	0.67	11.2
averages		0.77	0.39	0.42	0.56	0.42	0.25	0.53	0.62	3.04	0.12	0.54	0.37	0.65	10.63
mean errors		0.04	0.01	0.02	0.02	0.03	0.02	0.03	0.02	0.79	0.01	0.07	0.03	0.04	1.67

[1] No MASS data are available for the UH site.

Figure 1 illustrates the results for the DIMM and MASS fits that have the smallest and the largest χ^2 per degree of freedom. Log-log displays allow visualizing the shapes of these distributions over large density ranges and trace an inverted parabola centred on the median $\log(<\varepsilon_0>)$ for pure log-normal distributions. The figure shows that two-components models can reproduce the data quite well over a range of more than four orders of magnitudes in density. The DIMM plot for Las Vizcachas is a good example of a distribution compressed on its better seeing side by a strong narrow component.

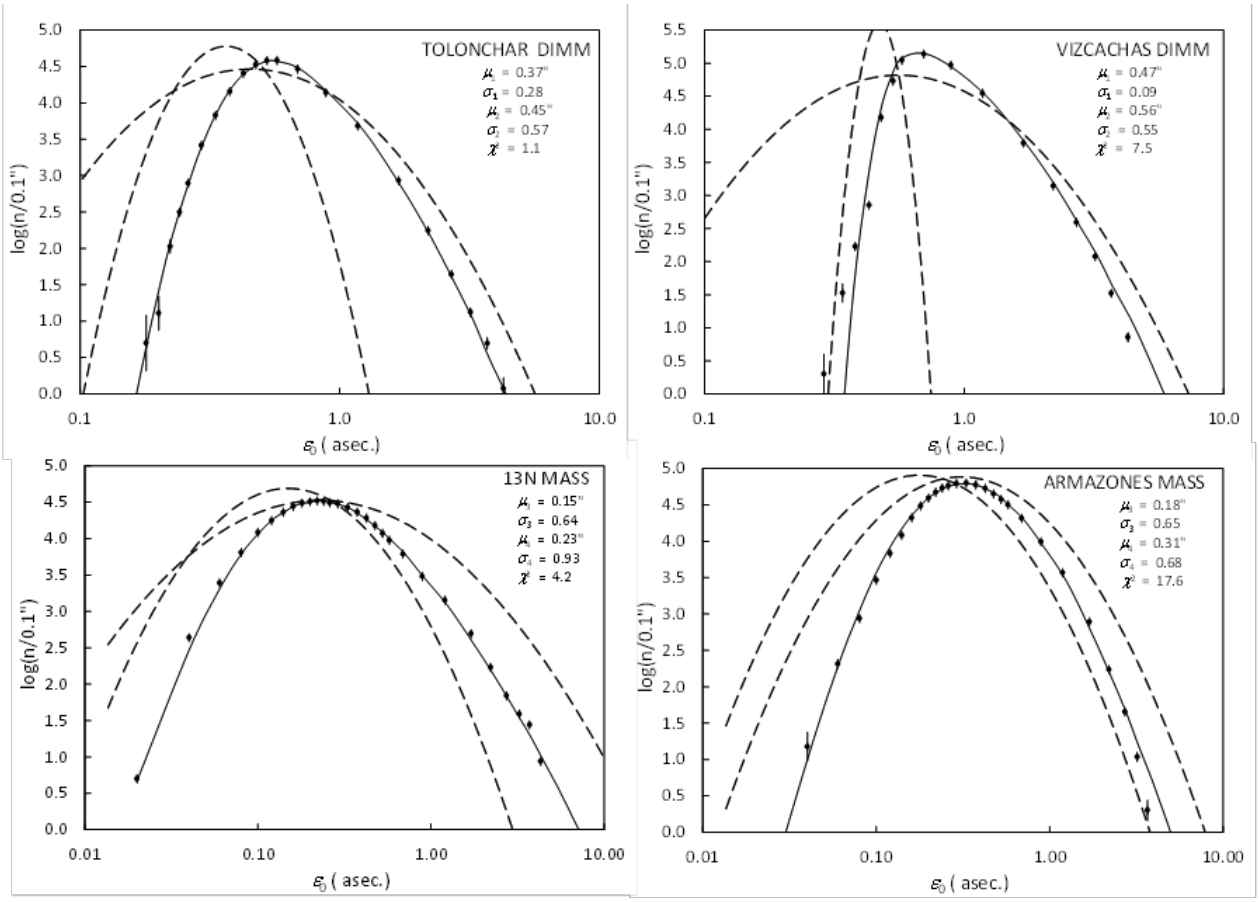

Fig 1 – These show the best (left) and the worst (right) two-component (dashed lines) fits to distributions of DIMM (above) and MASS (below) seeing values.

A detailed discussion of the relations between the DIMM and MASS components is beyond the scope allowed by this paper. Important clues are that, as can be seen in table 1, the strong MASS components and the wide DIMM components have comparable dispersions and must be related. But, figure 2 shows that the strength μ_2 of the wide DIMM component is generally stronger than that the MASS strong component, very much so for some sites. This indicates that the wide DIMM component includes, in addition to the MASS component, a large-dispersion contribution that arises below an altitude of 250 m and is therefore not sensed by the MASS. Those sites where this contribution is the strongest are known to have particularly strong low altitude turbulence [3] [4] [5].

All DIMM distribution models require the contribution of a narrow (σ_1 ~ 0.25) rather weak ($\mu_1 \sim 0.4$") component (figure 3). As figure 1 illustrates, these narrow component limits and steepens the better seeing side of the ε_0 distributions produced by turbulence at altitude and must arise by processes different from those that prevail in the upper atmosphere. In our model the components are additive. In contrast, the DIMM seeing above Dome C in Antarctica results from two or three *sporadic* turbulent components [6] [7], the surface layer being very dominant at times.

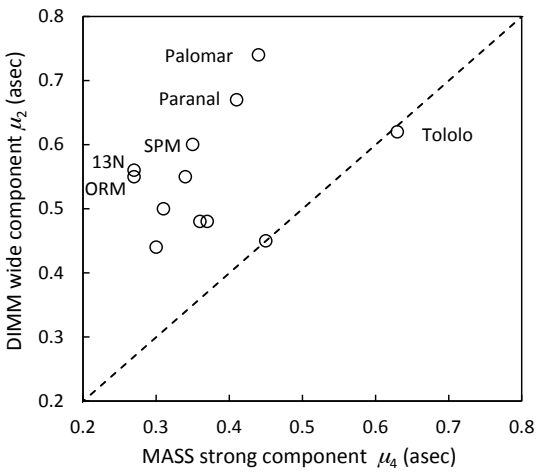

Fig 2 - The wide DIMM components are generally stronger than the strong MASS components.

It will have been noticed that in table 1 the χ^2 are generally much larger for the MASS fits than for the DIMM fits. This must be because at any site the DIMM always sample the full effect of the two components whereas the sensing of the high altitude, broader dispersion component by the MASS is variably contaminated by effect of the lower altitude turbulence. This variability generates additional noise in the shape of the distributions of MASS seeing values and lowers the χ^2 of the fits.

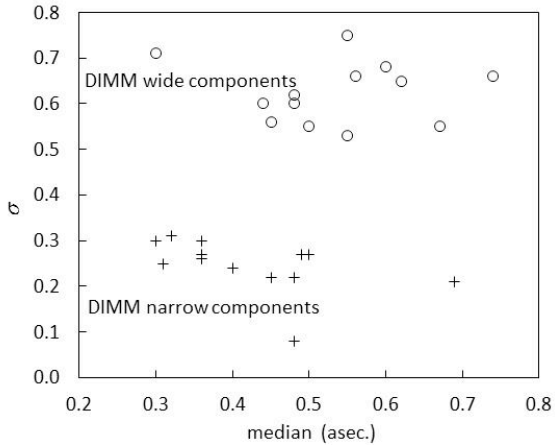

Fig. 3 – Models of DIMM seeing values distributions require the combined contributions of two components with notably different dispersions.

3. Seeing evolutions

Figure 4 shows DIMM seeing values sampled every minute over 10 consecutive summer nights at Mauna Kea 13N and Cerro Armazones. It says all there is to say about seeing evolution: "Seeing is a fickle friend: There is no such thing as a stable seeing night." More quantitative evidence will now be presented that forecasting seeing and successful "seeing sensitive" telescope scheduling are tall challenges.

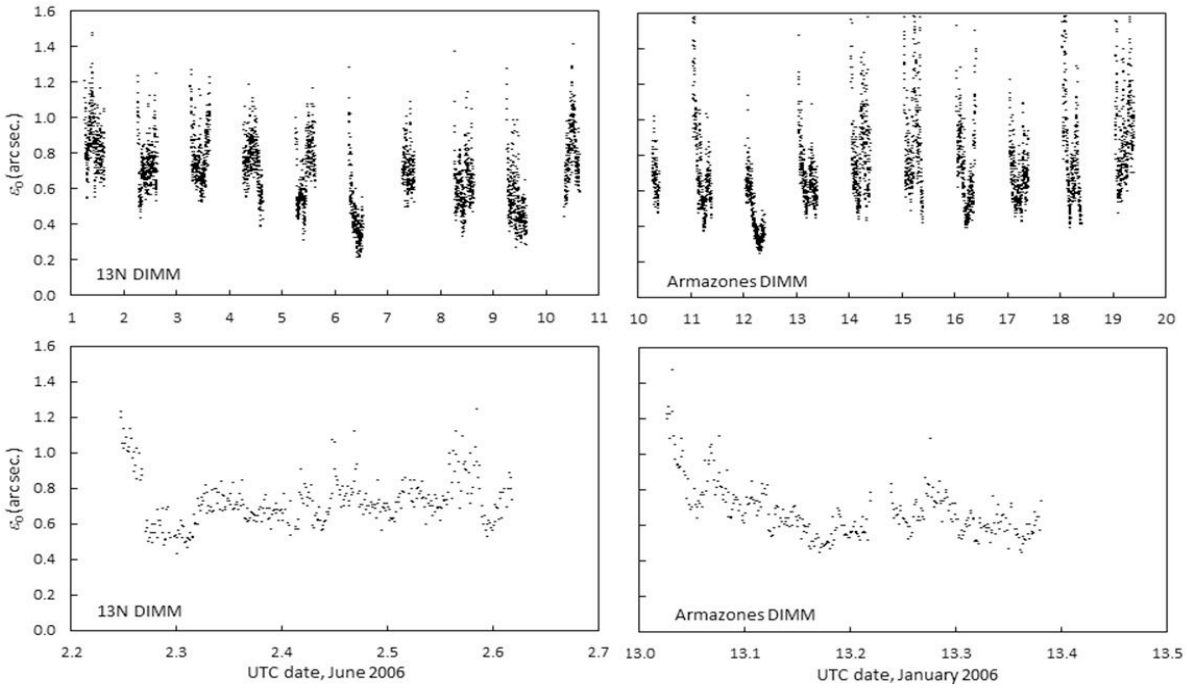

Fig. 4- Seeing is a fickle friend.

During a single night, seeing values typically span a range of a factor of 4 (figure 5). At Armazones, as at all good sites, DIMM seeing episodes better than 0.5" (telescopic image quality < 0.40" for L_0 = 30 m) occur on 80 percent of the nights.

Seeing evolution can be described by the time delay dependence of the seeing fractional difference *FD* as defined by Racine [8] and by Skidmore et al. [9]:

$$FD(\Delta t) \equiv |\varepsilon(t + \Delta t) - \varepsilon(t)|/(\varepsilon(t + \Delta t) + \varepsilon(t)). \quad (1)$$

The DIMM and MASS *FD* values for 2 sites are displayed against the delay Δt in figure 6. Such relations seeing were generated for all sites and for seeing values ranging from ¼ to 4 times the median values. The delays required for *FD* to reach 0.1 are shown as a function of the prevailing seeing in figure 7. The most stable seeing is the modal seeing. At the 10th and 90th percentiles of the distributions the seeing evolves two times faster. The maximum values for each site are given in table 2. The seeing speeds differ significantly between sites.

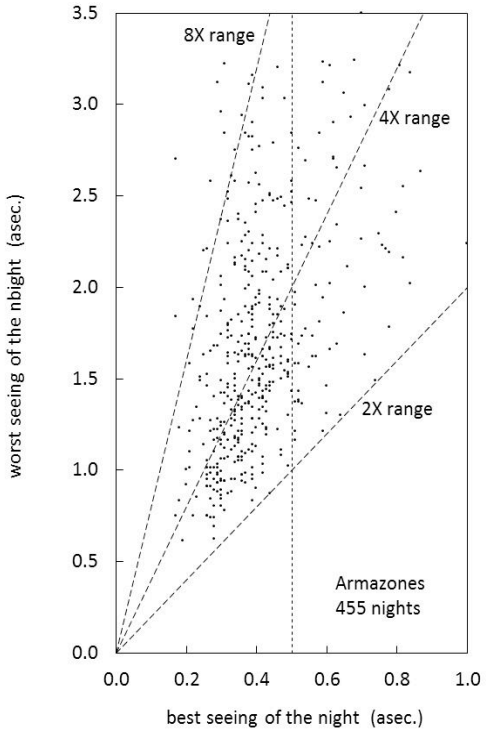

Fig. 5 – The best and worst seeing values for 455 Armazones nights are compared.

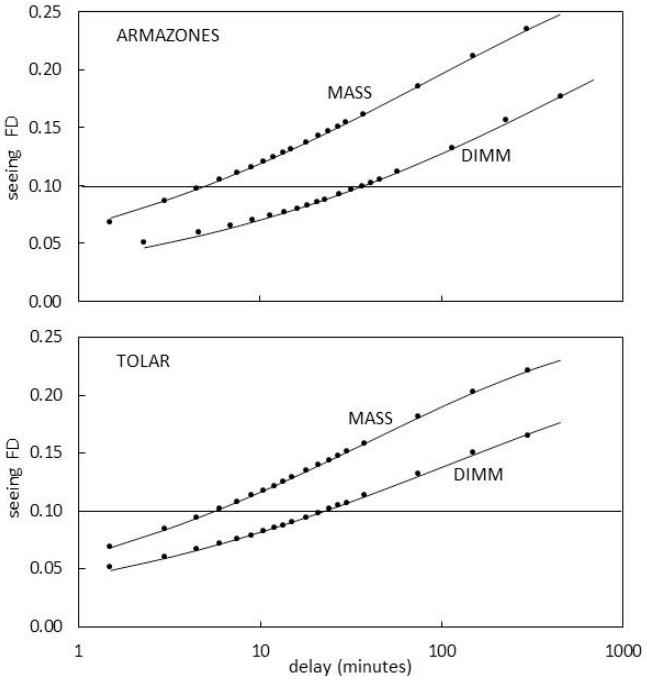

Fig. 6 – These show the evolutions of the fractional seeing differences with time delay for 2 sites.

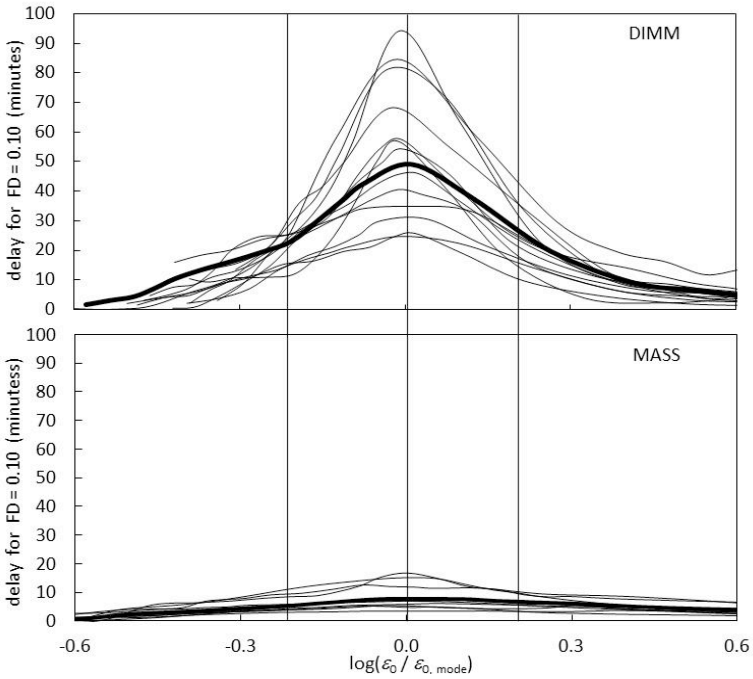

Fig. 7 – The delays for the fractional differences to reach 10 percent are plotted against the prevailing seeing values for each site. The bold curves are the average relations. The vertical lines are at the 10th, 50th and 90th percentiles of the seeing values distributions.

4. Conclusion

At all sites studied, the density distributions of DIMM and MASS seeing values can be satisfactorily reproduced over density ranges that reach four orders of magnitude by random combinations of the seeing values from two independent equal-population log-normal seeing components. The wider of these components is stronger than the integrated turbulence sensed by a MASS and includes the effects of optical turbulence below an altitude of 250 m. The narrower and weaker DIMM probably arises at low elevation.

Table 2 : Maximum Delays for 10% *FD*

Sites	DIMM (minutes)	MASS (minutes)
Pachon	94	7
Palomar	85	16
Vizcachas	81	17
Tololo	68	13
SPM	57	22
UH	57	--
Tolonchar	54	6
Armazones	46	5
Tolar	41	8
Paranal	35	15
13N	31	3
CFHT	26	4
ORM	25	5

The statistical evolutions of seeing values differ markedly between nights and between sites. There is no such thing as a stable seeing night. The seeing varies typically by a factor of 4 throughout a night. At good sites, the seeing from an elevation of 7-m above grade reaches sub-half-arc second on 80% of the night. It is most stable when near its modal value where the average time for a 10% change in DIMM seeing is ~50 minutes; it is ~25 minutes at the 10^{th} and 90^{th} percentiles of the distributions. The MASS seeing evolves ~7 times faster than the DIMM seeing on average. These lifetimes vary by a factor of 4 between the fastest and the slowest seeing sites.

5. References

[1] Sarazin M & Roddier F 1990 *A&A* **227** 294
[2] Kornilov V, Tokovinin A, Vozyakova O, Zaitsev A, Shatsky N, Potanin S & Sarazin M 2003 *SPIE* **4839** 837
[3] Sarazin M, Melnick J, Navarrete J. & Lombardi G 2008 *New Facts about the Evolution of Seeing at Paranal*, ESO Messenger **132** 11
[4] Tokovinin A, Bustos E & Badja . 2010 MNRAS **404** 1186
[5] Els S, Travoullion T, Schöck M, Riddle R, Skidmore W, Seguel J, Bustos E & Walker D 2009 *Pub. Astron. Soc. Pacific* **121** 527
[6] Fossat E, Aristidi E, Agabi K. Bondoux E, Challita Z, Jeanneaux F & Mekarnia D 2010 *A&A* **517** 69
[7] Aristidi E, Fossat E, Agabi A, Mékarnia D, Jeanneau F, Bondoux E, Challita Z, Ziad A, Vernin J & Trinquet H 2009 *A&A* **499** 955
[8] Racine R 2005 *Pub. Astron. Soc. Pacific* **117** 401
[9] Skidmore W, Els S, Travouillon T, Riddle R, Schöck M, Bustos E, Seguel J & Walker D 2009, *Pub. Astron. Soc. Pacific* **121** 115

Acknowledgements

This study was made possible thanks to colleagues who provided access to gigabytes of DIMM and MASS data: CFHT Billy Mahoney, ESO Marc Sarazin, NOAO Andrei Tokovinin, IAC Casiana Muños-Tuñón, TMT Mathias Schöck and Warren Skidmore and UH Mark Chun. Their help is gratefully acknowledged. Perceptive and encouraging comments on earlier versions of this work by Elena Masciadri, Andrei Tokovinin and Marc Sarazin help devising a more realistic and, hopefully, clearer analysis. Mark Sarazin kindly presented this paper at the Durham 2014 "Adapting to the Atmosphere" Conference when its author was unable to do so.